nature biotechnology

Drug sensitivity of single cancer cells is predicted by changes in mass accumulation rate

Mark M Stevens[1,2,14], Cecile L Maire[3,14], Nigel Chou[1,4,14], Mark A Murakami[3,14], David S Knoff[3], Yuki Kikuchi[1,5], Robert J Kimmerling[1,4], Huiyun Liu[3], Samer Haidar[3], Nicholas L Calistri[1], Nathan Cermak[6], Selim Olcum[1], Nicolas A Cordero[3], Ahmed Idbaih[7,8], Patrick Y Wen[9], David M Weinstock[3,10], Keith L Ligon[3,10–12] & Scott R Manalis[1,4,13]

Assays that can determine the response of tumor cells to cancer therapeutics could greatly aid the selection of drug regimens for individual patients. However, the utility of current functional assays is limited, and predictive genetic biomarkers are available for only a small fraction of cancer therapies. We found that the single-cell mass accumulation rate (MAR), profiled over many hours with a suspended microchannel resonator, accurately defined the drug sensitivity or resistance of glioblastoma and B-cell acute lymphocytic leukemia cells. MAR revealed heterogeneity in drug sensitivity not only between different tumors, but also within individual tumors and tumor-derived cell lines. MAR measurement predicted drug response using samples as small as 25 μl of peripheral blood while maintaining cell viability and compatibility with downstream characterization. MAR measurement is a promising approach for directly assaying single-cell therapeutic responses and for identifying cellular subpopulations with phenotypic resistance in heterogeneous tumors.

The choice of drug regimens for individual cancer patients has historically been based on treatment responses observed in large studies across heterogeneous populations. The shortcomings of this approach have motivated a broad effort to personalize treatment decisions for each patient based on the presence or absence of genetic, epigenetic or other biomarkers in an individual tumor[1,2]. Although population-based studies have been successful in some instances (e.g., in lung cancers with mutations of *EGFR* or rearrangements involving *ALK*), the vast majority of cancer therapeutics have no known markers for susceptibility or resistance[3]. Even when marker-based predictions can be made, they do not guarantee patient response, as many are the result of correlations from population-based studies[4,5].

The second major shortcoming of nearly all available biomarkers is that they are derived from analyses of bulk tumor populations, and therefore do not predict the emergence of resistant subpopulations. More sensitive approaches of genetic characterization, such as single-cell sequencing, are becoming increasingly common as research platforms, but are not yet amenable to a clinical setting[6,7]. These approaches also suffer from the same shortcoming as bulk assays, that is, the lack of predictive genetic or transcriptional markers.

In contrast with most biomarkers, functional assays can provide phenotype-driven predictors of therapeutic response that represent the integrated output of multiple parameters, including genetic, epigenetic, environmental and other variables that determine response. Detection of clinical response in a patient following treatment initiation is currently measured either by imaging to quantify bulk tumor volume or by directly measuring tumor burden within a compartment (e.g., peripheral blast counts). However, these assessments are delayed in time (ranging from days to months), and clinical indicators are only useful for making *post hoc* treatment decisions. In the ideal scenario, therapeutic functional assays would be used to guide selection of treatment that would induce response and thereby avoid problematic side effects from inefficacious therapies.

Although functional assays are essential clinical tools for assessing the antibiotic susceptibility of microbes, no such approaches have been widely adopted for patients with cancer[8,9]. Existing platforms to measure cancer cell growth, such as ATP-based assays (CellTiter-Glo), require extended time in culture and a large number of tumor cells[10]. This precludes their use for the large majority of patients, who have limited amounts of cancer tissue available. Furthermore, these bulk

[1]Koch Institute for Integrative Cancer Research, Massachusetts Institute of Technology, Cambridge, Massachusetts, USA. [2]Department of Biology, Massachusetts Institute of Technology, Cambridge, Massachusetts, USA. [3]Department of Medical Oncology, Dana-Farber Cancer Institute, Harvard Medical School, Boston, Massachusetts, USA. [4]Department of Biological Engineering, Massachusetts Institute of Technology, Cambridge, Massachusetts, USA. [5]Hitachi High-Technologies Corporation, Ibaraki-ken, Japan. [6]Program in Computational and Systems Biology, Massachusetts Institute of Technology, Cambridge, Massachusetts, USA. [7]Inserm U 1127, CNRS UMR 7225, Sorbonne Universités, UPMC Univ Paris 06 UMR S 1127, Institut du Cerveau et de la Moelle épinière, ICM, Paris, France. [8]AP-HP, Hôpitaux Universitaires La Pitié Salpêtrière - Charles Foix, Service de Neurologie 2-Mazarin, Paris, France. [9]Center For Neuro-Oncology, Dana-Farber Cancer Institute, Harvard Medical School, Boston, Massachusetts, USA. [10]Broad Institute, Cambridge, Massachusetts, USA. [11]Department of Pathology, Boston Children's Hospital, Boston, Massachusetts, USA. [12]Department of Pathology, Brigham and Women's Hospital, Boston, Massachusetts, USA. [13]Department of Mechanical Engineering, Massachusetts Institute of Technology, Cambridge, Massachusetts, USA. [14]These authors contributed equally to this work. Correspondence should be addressed to S.R.M. (srm@mit.edu), D.M.W. (davidm_weinstock@dfci.harvard.edu) or K.L.L. (keith_ligon@dfci.harvard.edu).

Received 23 November 2015; accepted 30 August 2016; published online 10 October 2016; doi:10.1038/nbt.3697

approaches are ill-suited for characterizing therapeutic susceptibility of subpopulations that exist in heterogeneous tumors[10].

An ideal functional assay for predicting therapeutic response in patients with cancer would accurately measure responses to both single drugs and drugs in combination; require minimal sample input; avoid artifacts that result from long-term, *in vitro* culture; quantify therapeutic response at the single-cell level; return results in a time frame that is conducive to therapeutic decision making; and maintain cell viability to allow for downstream functional and molecular interrogations.

We developed an approach for functionally assessing the therapeutic sensitivity of single cancer cells by weighing each cell repeatedly over a 15-min period in a suspended microchannel resonator (SMR) (**Fig. 1a**)[11–13], either in the presence or absence of cancer therapeutics. Resonator-based approaches have been used to measure an array of cellular physical properties[14] and, in one preliminary study, response to therapeutics[15]. Following the incubation of tumor cells with drug, the SMR was able to detect changes in the growth of single cells to predict therapeutic response without the need for extended culture. To validate this approach, we applied the SMR to traditional cancer cell lines, patient-derived cell lines (PDCLs) and primary leukemia cells.

RESULTS

MAR measurement

The SMR is a cantilever-based microfluidic mass sensor that measures the buoyant mass (referred to hereafter simply as mass) of live single cells with a resolution near 50 fg, which is highly precise given that the average buoyant mass of a hematopoietic cell is ~75 pg[12]. Cells were measured in suspension while under culture conditions, with controlled media temperature and CO_2 concentration to maintain cell viability and growth[13]. A series of mass measurements was made on an individual cell every ~30 s for ~15 min, allowing for determination of the MAR, which was defined as the change in mass over time (**Fig. 1a**)[12]. In addition to the MAR, we also used the absolute single-cell mass as a biomarker, which was determined for each cell during the MAR measurement. By measuring MAR on multiple cells from the same population, the SMR revealed heterogeneity in mass and MAR across the population, rather than an average of the tumor bulk. The degree to which mass and MAR behaved as independent biomarkers varied depending on conditions and cell type. Although linear discriminate analysis (LDA) maximized the predictive capability of these two biomarkers, we used a simplified metric of MAR normalized by mass for most of our experiments.

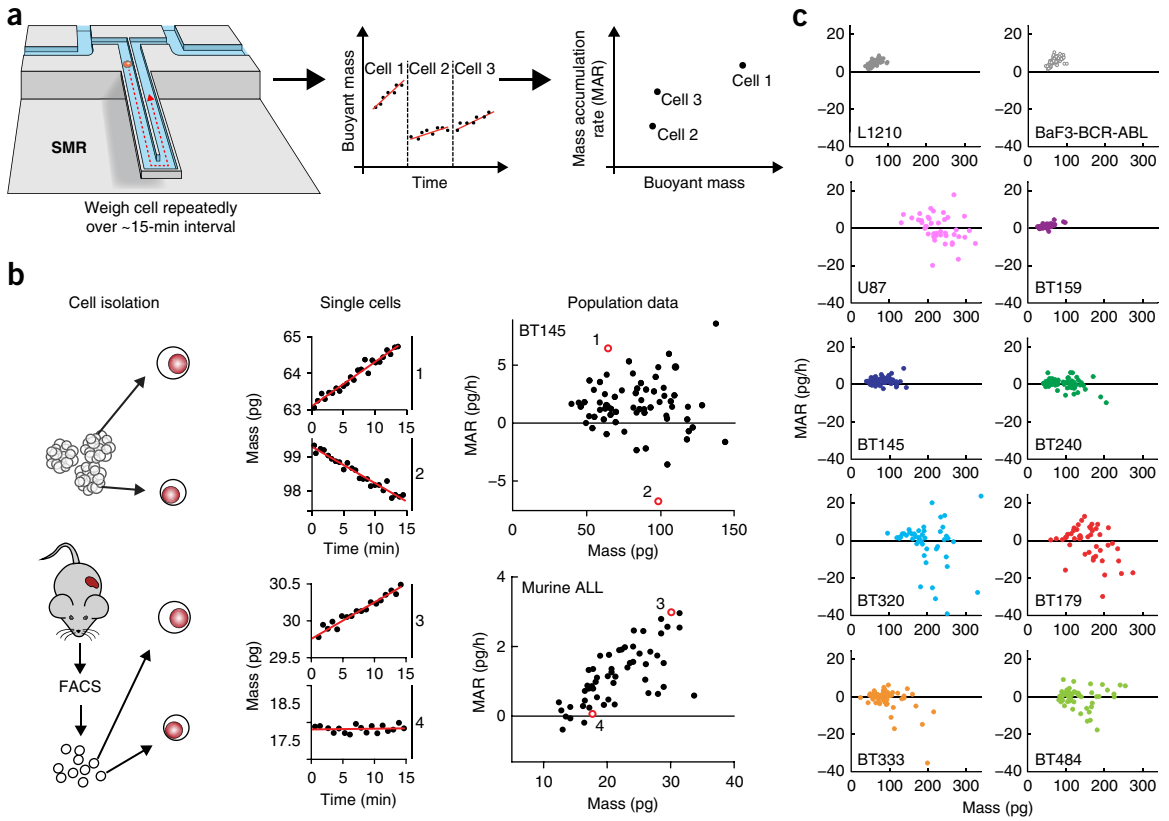

Figure 1 MAR measurements characterize single-cell heterogeneity in growth across GBM-PDCLs and conventional cell lines. (**a**) Schematic of workflow. Single cells were weighed repeatedly over a 15-min interval by iterative passage through the SMR device. A linear fit was applied to those measurements and the resulting data was plotted as MAR versus buoyant cell mass. (**b**) MAR measurements over ~15 min for single cells from the BT145 GBM PDCL (top) and primary BCR-ABL ALL cells directly isolated from mice (bottom). Cells were dissociated (for BT145) or purified by fluorescence-activated cell sorting (for ALL), and single cells were measured. The specific single-cell plots shown in the middle column are represented as red open circles along with other single cells (black dots) plotted as a function of mass. (**c**) MAR versus mass distributions from seven GBM-PDCLs, two conventional hematopoietic cell lines (L1210 and BaF3-BCR-ABL) and one conventional GBM cell line (U87) for comparison. Each GBM-PDCL plot includes measurements from three successive passages *in vitro* (**Supplementary Fig. 3**), and each dot represents a single cell. From left to right, row by row, $n = 84, 46, 44, 51, 52, 61, 48, 46, 64$ and 59 cells.

Single-cell MARs reveal tumor growth heterogeneity

To better characterize the platform's performance, we applied this method to two cancer cell types known to be viable and proliferate in suspended cell culture: glioblastoma (GBM) and acute leukemias. First, we analyzed a fast growing GBM-PDCL (BT145), which grows as free-floating 'stem-like' cells and tumorspheres, as well as primary leukemia cells isolated directly from mice with genetically engineered acute lymphoblastic leukemia (ALL) expressing the fusion protein BCR-ABL. Consistent with our previous findings[12], the SMR was able to quantify MAR of single cells over ~15-min intervals with high signal-to-noise ratios in both tumor types (**Fig. 1b**). During this time, the cells acquired less than a few picograms of biomass. This is equivalent to an increase in cell diameter on the order of only 10 nm.

To determine whether cell proliferation potential could be maintained after passage through the SMR, we isolated single BT145 GBM cells after MAR measurement and then assayed them for their ability to form tumorspheres. Overall, 14 (36%) of 39 single cells formed tumorspheres compared with 217 (45.2%) of 480 single cells isolated directly from a bulk culture ($P = 0.26$; **Supplementary Fig. 1**). Thus, MAR measurement had no statistically significant effect on viability or stem-like cell phenotype.

The heterogeneity of single-cell growth across cell lines or patient models has not been well characterized. In BT145 cells, MAR measurements enabled the delineation of different growth populations, identifying cells of both large and small mass with positive, zero and negative MAR (**Fig. 1b**). GBM tumors are known to harbor an exceptionally diverse admixture of growing, senescent, quiescent and dying cells[16,17]. Examination of BT145 by immunohistochemistry also confirms the presence of these heterogeneous properties in PDCLs (**Supplementary Fig. 2**). Thus, heterogeneity of MAR and mass in this line seems to parallel the known growth heterogeneity and morphological diversity of cells seen in primary GBMs. In contrast, almost all primary BCR-ABL ALL cells had positive MARs that monotonically increased with cell mass (**Fig. 1b**).

To determine the range of growth diversity that might exist across patients in a single tumor type, we measured MARs of single cells from seven different GBM-PDCLs with diverse genotypes (**Supplementary Table 1**) over three successive passages (**Supplementary Fig. 3**)[18]. MAR measurements revealed significant inter- and intra-PDCL heterogeneity across the seven PDCLs with single-cell diversity in both MAR and mass. These findings were in stark contrast with the homogeneity of MARs across conventional hematopoietic cell lines, such as the L1210 leukemia cell line and the murine lymphoblastoid BaF3 cell line, which was engineered to express BCR-ABL (BaF3 BCR-ABL) (**Fig. 1c**). Such homogeneity did not appear to be related to the advanced age and passage of these lines, as the conventional GBM cell line U87 exhibited significant MAR heterogeneity. Some lines, such as BT159 and BT145, had more homogenous patterns of cell proliferation, whereas BT320 and BT179 exhibited the most heterogeneous phenotypes, which we confirmed using immunohistochemistry analysis (**Supplementary Fig. 2**). The extent of growth heterogeneity in individual GBM-PDCLs was maintained across consecutive passages (**Supplementary Fig. 3**), suggesting that intra-tumoral diversity in growth is an inherent property of GBM PDCLs even during *in vitro* propagation.

MAR predicts cell line sensitivity to targeted therapy

To test the ability of MAR measurements to predict drug susceptibility in an established cell line, we used BaF3 cells that were engineered to express either wild-type BCR-ABL or the BCR-ABL T315I mutant, which is resistant to the tyrosine kinase inhibitor imatinib[19,20].

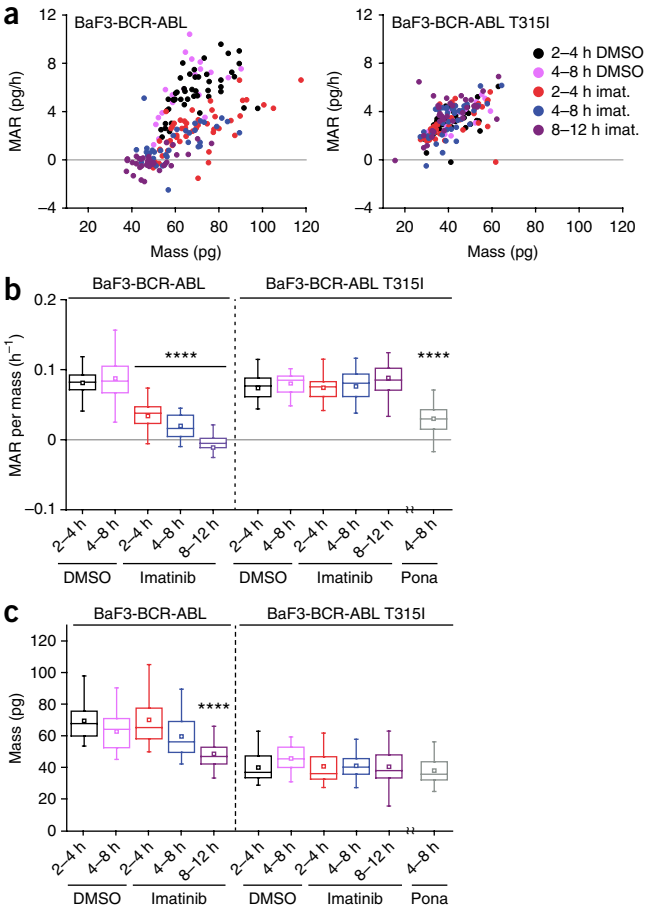

Figure 2 Murine BaF3 lymphoblastoid cells rapidly reduce MAR following exposure to active kinase inhibitors. (**a**) MAR versus cell mass of imatinib-sensitive BaF3-BCR-ABL or imatinib-resistant BaF3-BCR-ABL T315I cells exposed to 1 μM imatinib (imat.). (**b**,**c**) Data from **a** are shown as MAR per mass (**b**) or as a mass box-plot (**c**), and include BaF3-BCR-ABL T315I cells treated with 100 nM ponatinib. Boxes represent the inter-quartile range and white squares represent the average of all measurements. *P* values were calculated using the non-parametric Mann-Whitney *U* test, comparing treatment groups to DMSO for the same treatment duration. ****$P < 0.0001$ in highlighted segments. Time points were taken on at least three biological replicate cultures on different days. From left to right, $n = 46, 20, 48, 37, 36, 42, 15, 41, 27, 41$ and 41 cells.

Treatment of BaF3-BCR-ABL cells with imatinib at the therapeutically achievable concentration of 1 μM for only 2–4 h significantly decreased MAR without altering the distribution of mass (**Fig. 2**). With longer durations of exposure to imatinib, the reduction in MAR became more pronounced (**Fig. 2b**) and cell mass was reduced (**Fig. 2c**). When we applied the same conditions to BaF3-BCR-ABL T315I cells, we observed no significant change in MAR or mass distributions (**Fig. 2**). However, exposure of these cells to the third-generation tyrosine kinase inhibitor ponatinib, which retains activity against BCR-ABL T315I, recapitulated the same reduction in MAR that we observed following imatinib treatment of BaF3-BCR-ABL cells (**Fig. 2b**)[20]. Thus, MAR can distinguish therapeutic susceptibility from resistance in single BaF3 cells after only a few hours of drug exposure.

Next, we tested the ability of MAR measurements to predict therapeutic susceptibility when applied to GBM- PDCLs that had heterogeneous and complex MAR profiles, including cycling (non-G0) as well as non-cycling cells (G0) (**Fig. 1** and **Supplementary Fig. 2**)[16,17].

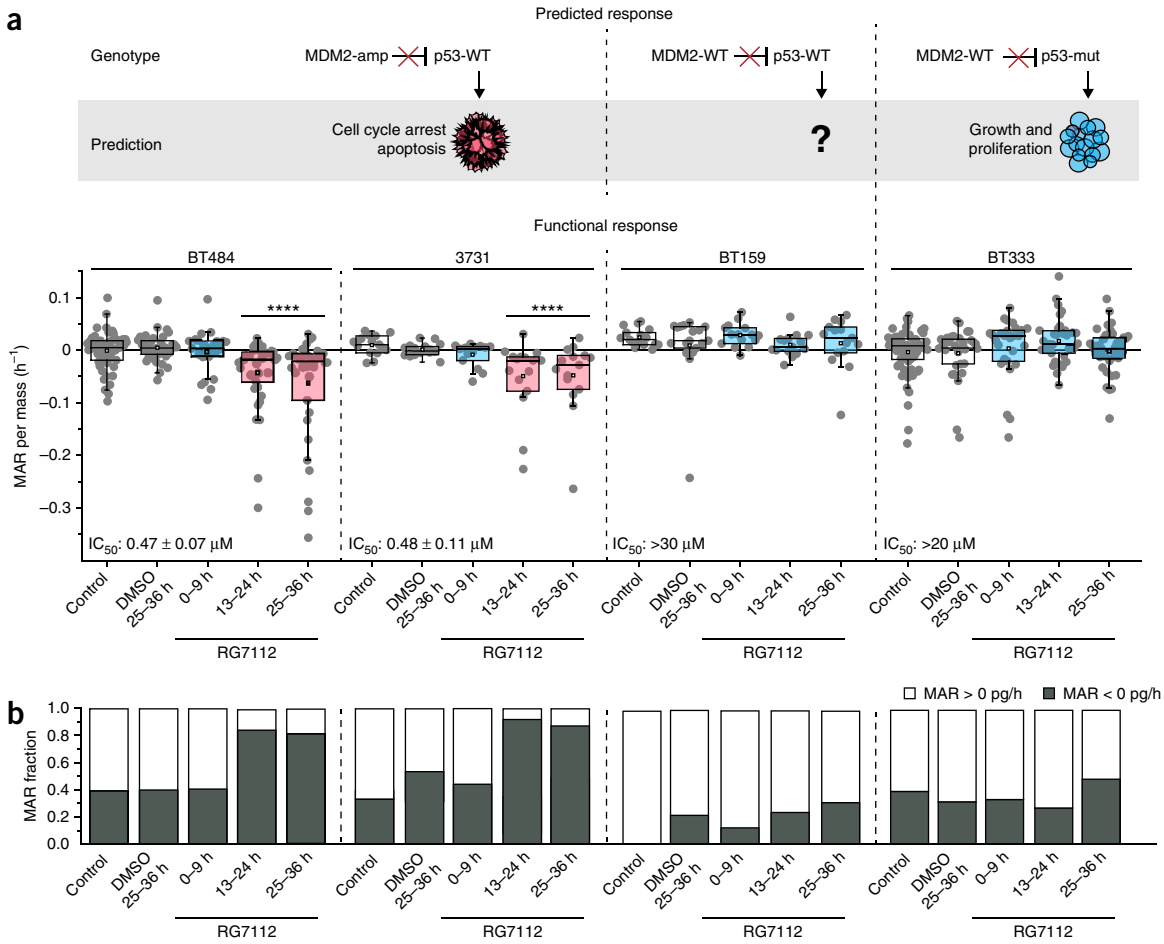

Figure 3 MAR predicts sensitivity of human GBM-PDCLs to targeted therapy. (**a**) The expected response to RG7112 is outlined above each cell line, with the red 'X' indicating the drug's ability to block the inhibition of p53 signaling by MDM2. The measured functional responses of BT484, 3731 (*MDM2* amplified, *TP53* wild type (WT)), BT159 (*MDM2* WT, *TP53* WT) and BT333 (*MDM2* WT, *TP53* mutated) PDCLs to DMSO or the MDM2 inhibitor RG7112 at a therapeutically relevant concentration of 1 μM over 36 h are shown. Half-maximal inhibitory concentration (IC_{50}) data from 72-h CellTiter-Glo measurements are shown for reference. Complete data are shown in **Supplementary Figure 5**. Boxes represent the inter-quartile range and white squares represent the average of all cells. Gray circles show values for individual cells. *P* values were calculated using the non-parametric Mann-Whitney *U* test, comparing treatment groups to the DMSO control. $^{****}P < 0.0001$ for highlighted segments. Time points were taken on biological replicate cultures on different days. From left to right, $n = 59, 37, 25, 38, 37; 16, 18, 15, 15, 15; 15, 16, 14, 16, 15: 69, 32, 27, 37$ and 38 cells. (**b**) Data from **a** showing that the fraction of BT484 and 3731 cells with negative MARs increased following exposure to RG7112, but remained unaffected in BT159 and BT333 cells.

GBM is highly resistant to most therapeutics, but we previously reported that some GBM-PDCLs are sensitive to targeted *MDM2* inhibition[21]. In bulk tumors and cultures, MDM2 inhibitors are known to induce responses in cells in which wild-type *TP53* is expressed and *MDM2* expression is amplified, whereas cells with mutant or deleted *TP53* are completely resistant to MDM2 inhibitors. However, cells that express wild-type *MDM2* and wild-type *TP53* have unpredictable sensitivity to MDM2 inhibitors in GBM and other tumor cell types[22]. We used the MDM2 inhibitor RG7112, a compound that is being evaluated in clinical trials, to determine how single-cell MAR responses of four GBM-PDCLs across this spectrum of *MDM2* and *TP53* mutant backgrounds might empirically correspond with genetics and CellTiter-Glo bulk sensitivity measures[23]. BT484 and 3731 cells, in which wild-type *TP53* is expressed and *MDM2* expression is amplified, had primarily negative MARs after incubation with 1 μM RG7112 for 13–24 h (**Fig. 3** and **Supplementary Fig. 4**). With increasing time, the number of cells with negative MAR further increased for 25–36 h, at which point >80% of cells were losing mass in both PDCLs (**Fig. 3** and **Supplementary Fig. 4**). In comparison, BT333 cells, which express wild-type *MDM2* and mutant *TP53*, showed no significant change in MAR compared with a DMSO-treated control over 36 h of RG7112 exposure (**Fig. 3** and **Supplementary Fig. 4**).

Contrasting the predictable sensitivity and resistance of the aforementioned lines, the responses of cells expressing wild-type *MDM2* and *TP53*, was not clearly correlated with the MDM2 and TP53 genotype. For example, targeted and whole-exome sequencing of BT159 cells, which express wild-type *MDM2* and *TP53*, revealed no mutations or copy number alterations in *TP53*, *TP63*, *TP73*, *CDKN2A*, *MDM4*, mitochondrial apoptosis mediators or other p53-related genes that could mediate MDM2 inhibitor resistance. However, BT159 exhibited no evidence of single-cell response by 36 h using MAR measurements, similar to the complete resistance exhibited by *TP53*-mutant BT333 cells (**Fig. 3** and **Supplementary Fig. 4**). MAR measurements for all lines were consistent with the response in viability as measured by CellTiter-Glo after 72 h of RG7112 exposure (**Supplementary Fig. 5**).

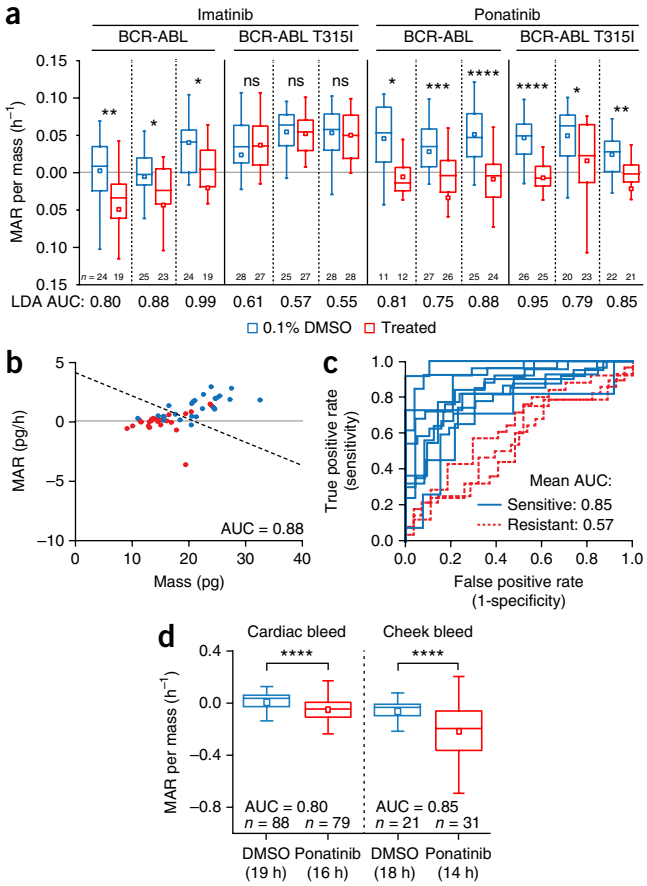

Figure 4 MAR distributions predict drug sensitivity of primary murine ALL cells to targeted therapy. (**a**) MAR per mass distributions of paired measurements from primary murine B-cell ALL (B-ALL) cells dependent on BCR-ABL or BCR-ABL T315I and treated with 1 μM imatinib, 100 nM ponatinib or DMSO. Measurements from individual mice are separated by a vertical dotted line. *n* indicates the number of cells for each measurement. AUC values for ROC curve of each paired data set are listed below the *x* axis. Boxes represent the inter-quartile range and white squares represent the average of all measurements. *P* values were calculated using the non-parametric Mann-Whitney *U* test, comparing treated cells to the DMSO control. (**b**) Representative MAR versus mass plot with overlay of an orthogonal vector (dotted line) designating the threshold resulting from LDA. (**c**) ROC curves of paired control and treatment data for each treatment replicate. Cells treated with therapy to which they were sensitive or resistant are shown with blue solid lines or red dotted lines, respectively. (**d**) MAR per mass distributions of paired measurements from primary murine B-ALL cells that were dependent on BCR-ABL. Cells isolated from the bloodstream of mice by either cardiac or cheek bleed and treated with 100 nM ponatinib or DMSO for the specified interval. *P* values were calculated using the Mann-Whitney *U* test, comparing treated cells to the DMSO control. $*P < 0.05$; $**P < 0.01$; $***P < 0.001$; $****P < 0.0001$. ns, not significant, $P > 0.05$.

MAR predicts primary cell sensitivity to targeted therapy

Next, we asked whether MAR measurements could effectively predict therapeutic response in primary tumor cells that were measured immediately after isolation from the *in vivo* setting. We harvested transgenic murine ALLs that expressed BCR-ABL or BCR-ABL T315I from the spleen of mice and used flow sorting to purify the leukemia cells (**Supplementary Fig. 6**)[24]. Single-cell MAR data was collected after 10–20 h of treatment with 1 μM imatinib or 100 nM ponatinib. Across three independent biological replicates, we observed a significant reduction in average MAR for leukemias expressing BCR-ABL following treatment with imatinib or ponatinib, as well as for leukemias expressing BCR-ABL T315I following treatment with ponatinib (**Fig. 4a**). By contrast, imatinib had no effect on leukemias expressing BCR-ABL T315I (**Fig. 4a**). We confirmed that BCR-ABL T315I leukemias were truly resistant to the imatinib analog nilotinib *in situ* by treating mice engrafted with these leukemias (**Supplementary Fig. 7**). In contrast with the marked effect of imatinib on MARs of wild-type BCR-ABL leukemia cells, exposure to imatinib *in vitro* for 24 h had no effect on the viability of leukemias expressing wild-type BCR-ABL in bulk culture, as determined by flow cytometry for annexin V and DAPI (**Supplementary Fig. 6**). Thus, the effect on MAR precedes these more standard metrics of drug response.

To gauge how robustly MAR measurements can predict primary ALL single-cell drug sensitivity, we generated a receiver-operating characteristic (ROC) after performing linear discriminate analysis (LDA) on each replicate's data set. Thus far, we had used the single metric of MAR per mass; however, we also considered MAR and mass as independently variable biomarkers. LDA projected the populations of the two-dimensional MAR versus mass data onto a single axis that provided the best ability to distinguish two populations, and then defined the ideal threshold for this classification (**Fig. 4b**). Subsequent ROC curve analysis was performed, and its area under the curve (AUC) was used as a metric of the ability to properly identify a single cell's classification as sensitive or resistant to therapy[25]. A random classifier has an AUC equal to 0.5, and a perfect classifier has an AUC of 1. The average AUC of non-selective conditions (DMSO-treated compared with imatinib-treated T315I leukemia) was 0.57, consistent with the expectation that resistant cells are indistinguishable from untreated cells (**Fig. 4a**,**c**). Under selective conditions, the ROC curves for MAR versus mass showed excellent resolution of sensitive and resistant populations, with an average AUC of 0.85 (**Fig. 4a**,**c**). ROC curves using mass or MAR as single parameters had significant power to classify single cells, but the single parameters were less consistent between replicates and were, on average, less accurate than using both parameters for classification (**Fig. 4c** and **Supplementary Fig. 8**).

MAR predicts sensitivity of circulating leukemia cells

Although GBM PDCLs and murine spleens essentially provided us with an unlimited number of tumor cells, we wanted to measure MARs from small samples, simulating the limited tissue available with patient biopsies. To this end, we isolated tumor cells from the peripheral blood of mice by cheek bleeding, which resulted in only 25 μl of total volume and did not compromise mouse survival. We performed these bleeds when circulating disease was as low as 4% of circulating mononuclear cells. This approach typically provided on the order of 10^3 total tumor cells for measurement following purification by flow sorting. To measure samples of low cell count and volume, we implemented a next-generation SMR array device that greatly simplified fluidic handling, increasing throughput by 20-fold and enabled the use of low-volume samples[26].

Single-cell MAR data was then collected on both cheek bleed (~25 μl) and cardiac bleed (~500 μl) samples that were exposed to either DMSO or 100 nM ponatinib for 14–20 h *in vitro*. Classification of single-cell drug response from cheek bleed samples (AUC = 0.85) were similar to those from splenocytes (AUC = 0.85) and cardiac bleed samples (AUC = 0.80) (**Fig. 4d** and **Supplementary Fig. 9**). The ability of MAR measurements to assay drug sensitivity of single cells isolated from very small amounts of blood makes it feasible to longitudinally screen for phenotypic resistance in individual patients through iterative sampling.

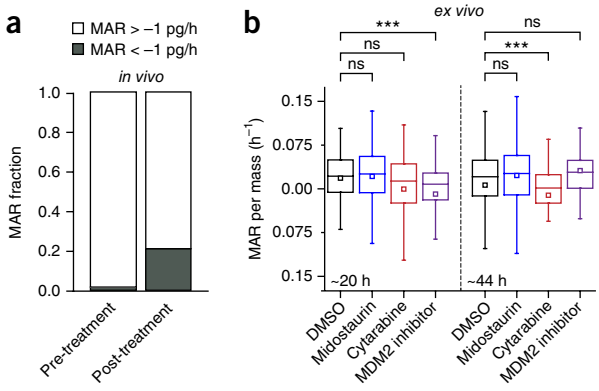

Figure 5 Patient samples treated *in vivo* or *ex vivo* show consistent reduction in MAR. (**a**) The fraction of cells with MAR of less than −1 pg/h from pre-treatment patient samples ($n = 86$ cells) and from samples obtained after the patient received 48 h of treatment with an experimental MDM2 inhibitor ($n = 95$ cells). MAR versus mass data for the same sample set is shown in **Supplementary Figure 10**. (**b**) Boxplots of MAR per mass of bone marrow leukemia cells treated *ex vivo* with either DMSO, 100 nM midostaurin, 1 µM cytarabine or an experimental MDM2 inhibitor and measured during 10-h windows centered around 20 and 44 h. Boxes represent the inter-quartile range and white squares the average of all measurements. *P* values were calculated using the non-parametric Mann-Whitney *U* test, comparing treated cells to the DMSO control. From left to right, $n = 137$, 102, 111, 78, 119, 103, 67 and 48 cells. ***$P < 0.001$. ns, not significant, $P > 0.05$.

Patient cells reduce MAR when treated *ex vivo* or *in vivo*

To define MAR assay compatibility with clinical samples, we ran two separate experiments using primary patient samples. First, we assayed ficolled peripheral blood samples from a patient with relapsed acute myeloid leukemia (AML). A sample obtained from the patient when they were not receiving treatment consisted largely of slightly positive MARs (**Fig. 5a** and **Supplementary Fig. 10**). After the patient had received 48 h of treatment with an experimental MDM2 inhibitor, a second peripheral blood sample was taken. This revealed a broader distribution of MARs compared with the pretreatment sample. Furthermore, a large population of cells with negative MARs of less than −1 pg/h appeared, indicating a shift in population MAR dynamics *in vivo* among the leukemia present in the peripheral blood (**Fig. 5a** and **Supplementary Fig. 10**). This shift toward negative MARs following treatment is consistent with our observations from *ex vivo* treatment of susceptible GBM-patient-derived cell lines (**Fig. 3**) and murine primary cells (**Fig. 4**).

Finally, we performed *ex vivo* treatment of a patient sample analogous to the approach applied to primary murine samples. Bone marrow leukemia cells from a patient presenting with newly diagnosed mutated-FLT3-positive AML with myelodysplastic-syndrome-related changes was treated in media with a range of therapeutics, including DMSO, 1 µM cytarabine (cytotoxic chemotherapy), 100 nM midostaurin (FLT3 and multikinase inhibitor) and an experimental MDM2 inhibitor (**Fig. 5b**). These cultures were incubated, and we measured MARs on three next-generation SMR array devices in parallel during 10-h windows that centered on 20 and 44 h. Cells in midostaurin showed no significant change in their distribution of MAR as compared to a DMSO control, consistent with the limited activity of single-agent midostaurin in FLT3-mutated AML[27]. In comparison, cytarabine did result in a reduction in MAR that was highly significant ($P = 0.00015$) at 48 h as compared with the control. Finally, cells treated with the experimental MDM2 inhibitor showed reduced MAR at 24 h, which rebounded by 48 h, potentially indicating a brief period of p53 target induction that is followed by the rapid induction of adaptive resistance.

DISCUSSION

We developed a functional assay for assessing single cancer cell therapeutic sensitivity based on measurements of MAR and the mass of individual cells. We validated the predictive power of combining MAR and mass measurements by confirming susceptibility or resistance of genetically defined cell lines, human GBM-PDCLs and primary murine ALLs in response to targeted therapeutics. In addition, by measuring mass accumulation rates of single cells across a population and establishing a growth profile for different GBM-PDCLs and cell lines, we have shown the heterogeneity of single-cell growth both in and across these populations. Additional experiments will be needed to prove the utility of MAR measurements for clinical decision-making. However, our initial data with primary patient leukemia samples, treated either *ex vivo* or *in vivo*, revealed responses that were consistent with our previously assayed *in vivo* models.

MAR measurement in the SMR is not a terminal assay, as cells are kept viable throughout the measurement and thereby remain compatible with downstream analyses. Thus, a key advantage of MAR measurements is that cells can be studied downstream of the SMR using other single-cell assays, as we demonstrated by quantifying the tumorsphere-forming potential of GBM-PDCL cells after passage through the device (**Supplementary Fig. 1**). This ability will ultimately allow for correlations between single-cell changes in MAR, other functional outcomes and non-functional biomarkers (e.g., genetics, gene expression and chromatin modifications). Further studies are needed to assess the effects of passage through the SMR on aspects of tumor cell biology, including changes in the transcriptome, genome and proteome. Previous studies have found that cellular and genomic properties of single cells can be measured using techniques such as RNA sequencing and are well-preserved following exposure to microfluidic environments[28].

Recent studies have used other functional approaches to predict therapeutic sensitivity of individual cancers. For example, one group used standard proliferation-based assays to quantify therapeutic susceptibilities of bulk cultures of PDCLs[10]. The results from this *ex vivo* screening predicted the response of *in vivo* xenografts to combination therapies. However, cell-to-cell heterogeneity is not captured by population approaches, and the utility of this strategy for clinical decision-making is limited by the months of prolonged culture required for PDCL creation.

Another recent study presented a functional approach called 'dynamic BH3 profiling', in which therapeutics are applied to cell lines or clinical tumor isolates, and then the percentage of cells that undergo mitochondrial outer membrane permeabilization (MOMP) is measured after introduction of a pro-apoptotic BH3 peptide[29]. Dynamic BH3 profiling robustly predicted which patients would respond to a given therapy across multiple cancer types. However, this approach requires cell permeabilization, which complicates the application of both downstream assays and phenotype validation, and does not clearly distinguish between subsets of cells with phenotypic heterogeneity.

MAR measurement addresses many of these limitations by assessing therapeutic susceptibility in single, live cells without the need for PDCL generation, but is subject to its own set of constraints. Most notably, *in vitro* culture is still necessary for a length of time adequate to elicit a growth response to applied therapeutics. In BaF3 cells, this occurred within 2–4 h, but GBM cells required longer culture to appreciably change MAR in the presence of MDM2 inhibition. Thus, the MAR measurement can reduce, but does not completely eliminate, the time in *in vitro* culture. In addition, the SMR currently requires cells to be in a single-cell suspension or small clumps for mass

and MAR measurement. Future studies will need to explore the utility in solid tumor systems, where the extent of dissociation required may perturb cellular viability and/or response. MAR measurements also initially suffered from low throughput. However, single-cell mass and MAR can now be obtained with a throughput exceeding 60 cells per h per device without sacrificing precision[26].

Perhaps the most important shortcoming of our approach, and the vast majority of functional assays, is a potential bias toward assessing only cell-intrinsic drug susceptibility. Microenvironmental interactions are known to influence *in vivo* drug response, but cellular 'memory' of these interactions may degrade during the course of *ex vivo* treatment[9]. There have been recent advancements in this arena involving implantable devices, but these approaches are currently only compatible with solid tumors and require tumors of a minimum size that are easily accessible[30]. To address the role of microenvironmental interactions, future studies using MAR measurements should explore whether alternative culture conditions can help to address the contribution of cell-extrinsic factors under controlled conditions; for example, tumor cells could be maintained *in vitro* in the presence of both drug and co-culture with stromal and/or immune cells before measurement. Alternatively, patient drug response *in situ* could be monitored. For example, patient tumor cells could be analyzed with MAR measurements immediately before and hours to days after treatment to help inform pharmacokinetics and pharmacodynamics. In fact, we applied this approach to a patient with AML (**Fig. 5**) to assess overall feasibility for clinical scenarios that could be explored in the future.

A substantial amount of work needs to be performed in the future to define the utility of mass and MAR as biomarkers for treatment response across disease types, in comparison with alternative functional assays, for drugs in combination, and across a wider range of drug mechanisms, where response may differ on the basis of the mechanism of cell death. However, given the scarcity of functional assays with the necessary characteristics to merit widespread application, MAR measurements in the SMR could be potentially useful as both a biological tool and a clinical platform.

METHODS

Methods and any associated references are available in the online version of the paper.

Note: Any Supplementary Information and Source Data files are available in the online version of the paper.

ACKNOWLEDGMENTS

These studies were supported by R01 CA170592 (S.R.M., K.L.L., P.Y.W.), P50 CA165962 (K.L.L., P.Y.W.), P01 CA142536 (K.L.L.) and R33 CA191143 (S.R.M., D.M.W.) from the US National Institutes of Health, U54 CA143874 from the National Cancer Institute (S.R.M.), and partially by Cancer Center Support (core) Grant P30 CA14051 from the National Cancer Institute, The Bridge Project, a partnership between the Koch Institute for Integrative Cancer Research at MIT and the Dana-Farber/Harvard Cancer Center (DF/HCC) (S.R.M., D.M.W.), and the Dana-Farber Cancer Institute Brain Tumor Therapeutics Accelerator Program (P.Y.W., K.L.L.). A.I. acknowledges support from Fondation ARC pour la Recherche sur le Cancer, The Institut Universitaire de Cancérologie, OncoNeuroThèque and the program Investissements d'avenir" ANR-10-IAIHU-06. M.M.S. acknowledges support from the NIH/NIGMS T32 GM008334, Interdepartmental Biotechnology Training Program grant. N. Chou acknowledges support from the National Science Scholarship, Agency for Science, Technology and Research (STAR), Singapore. D.M.W. is a Leukemia and Lymphoma Scholar. M.A.M. gratefully acknowledges support from the institutional research training grant T32 CA009172, from the National Cancer Institute.

AUTHOR CONTRIBUTIONS

N. Cermak, S.O. and S.R.M. designed devices. M.M.S., N. Chou, N. Cermak and S.O. designed and constructed the experimental setup. C.L.M., D.S.K., S.H., A.I., P.Y.W. and K.L.L. managed and created BT GBM-PDCLs. M.A.M. and H.L. managed and processed murine models of B-cell acute lymphocytic leukemia. M.A.M., H.L. and N.A.C. procured and processed patient samples. M.M.S., C.L.M., N. Chou, M.A.M., D.S.K., Y.K., N.L.C., N.A.C., N. Cermak, D.M.W., K.L.L. and S.R.M. designed the experiments. M.M.S., C.L.M., N. Chou, M.A.M., D.S.K., Y.K., R.J.K., H.L., S.H., N.L.C. and N.A.C. performed the experiments. M.M.S., C.L.M., N. Chou., M.A.M., D.S.K., Y.K., R.J.K., N.L.C., N. Cermak, N.A.C. analyzed the data. M.M.S., C.L.M., N. Chou, D.M.W., K.L.L. and S.R.M. wrote the paper with input from all of the other authors.

COMPETING FINANCIAL INTERESTS

The authors declare competing financial interests: details are available in the online version of the paper.

1. Mellinghoff, I.K. *et al.* Molecular determinants of the response of glioblastomas to EGFR kinase inhibitors. *N. Engl. J. Med.* **353**, 2012–2024 (2005).
2. Sos, M.L. *et al.* Predicting drug susceptibility of non-small cell lung cancers based on genetic lesions. *J. Clin. Invest.* **119**, 1727–1740 (2009).
3. Garraway, L.A. & Jänne, P.A. Circumventing cancer drug resistance in the era of personalized medicine. *Cancer Discov.* **2**, 214–226 (2012).
4. Klempner, S.J., Myers, A.P. & Cantley, L.C. What a tangled web we weave: emerging resistance mechanisms to inhibition of the phosphoinositide 3-kinase pathway. *Cancer Discov.* **3**, 1345–1354 (2013).
5. Haibe-Kains, B. *et al.* Inconsistency in large pharmacogenomic studies. *Nature* **504**, 389–393 (2013).
6. Navin, N. *et al.* Tumour evolution inferred by single-cell sequencing. *Nature* **472**, 90–94 (2011).
7. Francis, J.M. *et al.* EGFR variant heterogeneity in glioblastoma resolved through single-nucleus sequencing. *Cancer Discov.* **4**, 956–971 (2014).
8. Burstein, H.J. *et al.* American Society of Clinical Oncology clinical practice guideline update on the use of chemotherapy sensitivity and resistance assays. *J. Clin. Oncol.* **29**, 3328–3330 (2011).
9. Friedman, A.A., Letai, A., Fisher, D.E. & Flaherty, K.T. Precision medicine for cancer with next-generation functional diagnostics. *Nat. Rev. Cancer* **15**, 747–756 (2015).
10. Crystal, A.S. *et al.* Patient-derived models of acquired resistance can identify effective drug combinations for cancer. *Science* **346**, 1480–1486 (2014).
11. Burg, T.P. *et al.* Weighing of biomolecules, single cells and single nanoparticles in fluid. *Nature* **446**, 1066–1069 (2007).
12. Godin, M. *et al.* Using buoyant mass to measure the growth of single cells. *Nat. Methods* **7**, 387–390 (2010).
13. Son, S. *et al.* Direct observation of mammalian cell growth and size regulation. *Nat. Methods* **9**, 910–912 (2012).
14. Byun, S., Hecht, V.C. & Manalis, S.R. Characterizing Cellular Biophysical Responses to Stress by Relating Density, Deformability, and Size. *Biophys. J.* **109**, 1565–1573 (2015).
15. Wu, S. *et al.* Quantification of cell viability and rapid screening anti-cancer drug utilizing nanomechanical fluctuation. *Biosens. Bioelectron.* **77**, 164–173 (2016).
16. Lathia, J.D. *et al.* Direct in vivo evidence for tumor propagation by glioblastoma cancer stem cells. *PLoS One* **6**, e24807 (2011).
17. Deleyrolle, L.P. *et al.* Evidence for label-retaining tumour-initiating cells in human glioblastoma. *Brain* **134**, 1331–1343 (2011).
18. Cerami, E. *et al.* The cBio cancer genomics portal: an open platform for exploring multidimensional cancer genomics data. *Cancer Discov.* **2**, 401–404 (2012).
19. Pui, C.H., Relling, M.V. & Downing, J.R. Acute lymphoblastic leukemia. *N. Engl. J. Med.* **350**, 1535–1548 (2004).
20. Cortes, J.E. *et al.* Ponatinib in refractory Philadelphia chromosome-positive leukemias. *N. Engl. J. Med.* **367**, 2075–2088 (2012).
21. Verreault, M. *et al.* Preclinical efficacy of the MDM2 inhibitor RG7112 in MDM2-amplified and TP53 wild-type glioblastomas. *Clin. Cancer Res.* **22**, 1185–1196 (2015).
22. Jeay, S. *et al.* A distinct p53 target gene set predicts for response to the selective p53-HDM2 inhibitor NVP-CGM097. *eLife* **4** http://dx.doi.org/10.7554/eLife.06498 (published online 12 May 2015).
23. Andreeff, M. *et al.* Results of the phase I trial of RG7112, a small-molecule MDM2 antagonist in leukemia. *Clin. Cancer Res.* **22**, 868–876 (2016).
24. Lane, A.A. *et al.* Triplication of a 21q22 region contributes to B cell transformation through HMGN1 overexpression and loss of histone H3 Lys27 trimethylation. *Nat. Genet.* **46**, 618–623 (2014).
25. Pencina, M.J., D'Agostino, R.B. Sr., D'Agostino, R.B. Jr. & Vasan, R.S. Evaluating the added predictive ability of a new marker: from area under the ROC curve to reclassification and beyond. *Stat. Med.* **27**, 157–172, discussion 207–212 (2008).
26. Cermak, N. *et al.* High-throughput growth measurements on single cells via serial microfluidic mass sensor arrays. *Nat. Biotechnol.* http://dx.doi.org/10.1038/nbt.3666 (2016).
27. Fischer, T. *et al.* Phase IIB trial of oral Midostaurin (PKC412), the FMS-like tyrosine kinase 3 receptor (FLT3) and multi-targeted kinase inhibitor, in patients with acute myeloid leukemia and high-risk myelodysplastic syndrome with either wild-type or mutated FLT3. *J. Clin. Oncol.* **28**, 4339–4345 (2010).
28. Shalek, A.K. *et al.* Single-cell RNA-seq reveals dynamic paracrine control of cellular variation. *Nature* **510**, 363–369 (2014).
29. Montero, J. *et al.* Drug-induced death signaling strategy rapidly predicts cancer response to chemotherapy. *Cell* **160**, 977–989 (2015).
30. Jonas, O. *et al.* An implantable microdevice to perform high-throughput in vivo drug sensitivity testing in tumors. *Sci. Transl. Med.* **7**, 284ra57 (2015).

ONLINE METHODS

Cell culture of conventional cell lines. L1210, BaF3-BCR-ABL, and BaF3-BCR-ABL-T315I cells were maintained in suspension in RPMI-1640 media (Invitrogen, Cat#11875-119), supplemented with 10% FBS (Sigma-Aldrich, Cat#F4135), Penicillin-Streptomycin (Invitrogen, Cat#15140-122), and kept in a 37 °C, 5% CO_2, and humidified incubator. Cells were passaged every 2 d to 5 × 10^4 cells/ml, and used for SMR experiments between 24–36 h of growth at an approximate cell concentration of 2–4 × 10^5 cells/ml. L1210 cells were a gift from the Kirschner laboratory at Harvard University, and BaF3-BCR-ABL and BaF3-BCR-ABL-T315I were created from the parental BaF3 cell line obtained from the RIKEN BioResource Center. No further cell line validation was performed. All cell lines tested negative for mycoplasma.

For drug response experiments, cells in bulk were dosed for the specified interval with 0.1% DMSO, 1 μM imatinib (Santa Cruz Biotechnology, Cat#SC-202180), or 100 nM ponatinib (Selleckchem, Cat#AP24534). The cells were kept in drugged media during the measurements, and samples sizes were determined by practical limitations set by throughput.

Creation and cell culture of GBM PDCLs. GBM PDCLs were generated from patient tissue collected under an informed consent protocol (Dana Farber Harvard Cancer Center protocol #10-417) and two waived consent protocols (Dana Farber Harvard Cancer Center protocol #10-043 and Partner's Human Research Center protocol #2002 P000995). All protocols mentioned have been approved by Dana Farber Harvard Cancer Center and Partner's Human Research Center institutional review boards. Cells were harvested from excess tissue resection specimens through cycles of enzymatic (neural tissue dissociation kit with papain, Miltenyi) and mechanical dissociation in a tissue grinder (gentleMACS dissociator, Miltenyi). Cells were grown as tumorspheres in NeuroCult NS-A proliferation media (Miltenyi) supplemented with 2 μg/ml Heparin, 20 ng/ml human epidermal growth factor (EGF), 10 ng/ml human bFGF in ultra-low attachment coated flasks (Corning, Cat#3814), which were kept in a 37 °C, 5% CO_2, and humidified incubator. All PDCLs tested negative for mycoplasma.

Prior to loading in the SMR, the PDCLs were dissociated with Accutase (Sigma-Aldrich, Cat#A6964) at 37 °C for 7 min and plated as a single-cell population at 7–10 × 10^4 cells/ml. Tumorsphere forming assays were conducted by assessing the expansion of single-cells in a 96-well plate following 2 weeks of incubation, either isolated from the SMR, or as sorted by fluorescence-activated cell sorting (FACS).

For drug experiments, GBM-PDCLs were seeded into parallel cultures and treated with 1 μM of the MDM2 inhibitor RG7112 (Selleckchem), or DMSO. At each time point, one parallel culture was dissociated and immediately resuspended in drug media, and remaining parallel cultures were resuspended in fresh media with new drug. The dissociated cell suspensions were kept in drugged media during the measurements, and samples sizes were determined by practical limitations set by throughput.

Transgenic mouse model of BCR-ABL B-ALL. All animal experiments were performed with approval of the Dana-Farber Cancer Institute Institutional Animal Care and Use Committee. A transgenic mouse model of BCR-ABL B-ALL was generated by transplantation of lethally irradiated Ts1Rhr mice (B6.129S6-Dp(16Cbr1- ORF9)1Rhr/J; Jackson Laboratory; stock #005848) with syngeneic Hardy B cells transduced with an MSCV retrovirus coexpressing GFP and human BCR-ABL cDNA, as previously described[18]. For the present studies, 10^6 bulk splenocytes (P1 generation) were transplanted into lethally irradiated, wild- type, female, C57BL/6 mice at 6–8 weeks of age, which were followed daily for clinical signs of leukemia and sacrificed when moribund. Splenocytes or blood samples were harvested, subject to erythrocyte lysis (Qiagen, Cat#158904), and stained with an antibody targeting murine CD19 (Fisher Scientific, Cat#BDB551001). BCR- ABL B-ALL cells were isolated by sorting for CD19/GFP double-positive cells on a FACSAria II SORP fluorescence activated cell sorter (BD Biosciences).

For drug response experiments, sorted mouse leukemia cells were seeded at a density of 5 × 10^5/ml and cultured at 37 °C in a humidified 5% CO_2 incubator in RPMI (Gibco, Cat #11835055) supplemented with 10% FBS, 2 mM L-glutamine (Gibco, Cat#25030164), 50 μM 2-mercaptoethanol (Sigma, Cat#M3148), 50 IU/ml-50 μg/ml penicillin-streptomycin (Fisher Scientific, Cat#ICN1670049), 10 ng/mL recombinant murine IL-3 (PeproTech, Cat#213-13), 10 ng/ml recombinant murine IL-7 (PeproTech, Cat#217-17), 10 ng/ml recombinant murine stem cell factor (PeproTech, Cat#250-03), and 10 ng/ml recombinant murine FLT3-ligand (PeproTech, Cat#250-31L). Cells were kept in a 37 °C, 5% CO_2, and humidified incubator. Replicate cultures were dosed for 10 h with 0.1% DMSO, 1 μM imatinib (Santa Cruz Biotechnology, Cat#SC-202180), or 100 nM ponatinib (Selleckchem, Cat#AP24534). The cells were kept in drugged media during the measurements, which took place between 10–20 h of drug exposure, and samples sizes were determined by practical limitations set by throughput and measurement window length.

For *in vivo* confirmation of drug efficacy, female C57BL/6 mice were sublethally irradiated and transplanted with 7.5 × 10^5 murine leukemia cells harboring human BCR-ABL cDNA, of which 95% were BCR-ABL wild-type and 5% harbored the T315I allele. Upon engraftment, as defined by the presence of circulating leukemia at a level of 1–3% by peripheral blood flow cytometry, mice were treated with nilotinib 50 mg/kg/d via oral gavage (n = 2 mice). Nilotinib serves as a surrogate for imatinib, as both compounds have demonstrated activity against WT but not T315I BCR-ABL. Error bars represent s.d. Mice underwent serial BCR-ABL genotyping via the Sanger method to monitor the allelic frequency of BCR-ABL T315I.

Patient sample procurement and processing. Primary human leukemia specimens were collected from patients at the Dana-Farber Cancer Institute and Brigham and Women's Hospital upon provision of informed consent under one or more tissue banking protocols (Dana-Farber/Harvard Cancer Center protocols #01-206 and #11-104). Each protocol has been approved by the Dana-Farber/Harvard Cancer Center institutional review board. Peripheral blood and bone marrow samples underwent Ficoll density gradient centrifugation to enrich for mononuclear cells, followed by immunomagnetic enrichment of leukemia cells using CD33 MicroBeads (Miltenyi, Cat#130-045-501) if concomitant clinical testing indicated that tumor purity was <80%. Leukemia cells were seeded at 0.5–1.0 ×10^6/mL in DMEM supplemented with 15% FBS, 2 mM L-glutamine, 50 μM 2-mercaptoethanol, 50 IU/ml-50 μg/ml penicillin- streptomycin, and human cytokines SCF (100 ng/ml, PeproTech #300-07), IL3 (10 ng/ml, PeproTech #200-03), IL6 ((20 ng/ml, PeproTech 200-06), TPO (10 ng/ml, PeproTech #300-18), and FLT3-Ligand (10 ng/ml, PeproTech 300-19), as adapted from published methods[31]. For measurements of *in vivo* response, aliquots of cultured cells were immediately measured in the presence of DMSO or sustained drug pressure with the experimental MDM2 inhibitor. In the case of *ex vivo* treatment, aliquots were treated with an experimental MDM2 inhibitor, cytarabine (1 μM), midostaurin (100 nM), or DMSO (1:1,000) and were assessed using the SMR within 10-h windows centered on 20 and 44 h.

CellTiter-Glo assay. Cell viability in GBM neurospheres was assessed by quantification of ATP through chemiluminescence reading with CellTiter-Glo (Promega, Cat#G7570). GBM cells were plated as single cells at 2 × 10^3 cells/ml into wells of an ultra-low attachment coated 96-well plates (Corning, Cat#3474). In drug treatment experiments, viability was assessed at 72 h. All measurements were performed in triplicate according to manufacturer's protocol.

Measurement and operation of a SMR. The design and operation of the SMR have been previously described[11–14]. In short, single cells in suspension are passed through the SMR resulting in a frequency shift that is proportional to cell buoyant mass. The SMR can resolve the instantaneous rate of mass accumulation for a single cell in 15 min provided that the cell is weighed approximately every 30 s. Mass calculated from frequency shift using a calibration factor derived from measurements of frequency shifts of polystyrene beads with a known mass (Thermo Scientific, Cat#4208A). Mass versus time data of a single cell is then linearly fitted.

doi:10.1038/nbt.3697

For measurement in the SMR, cells were suspended in their standard growth media with or without drug. For GBM-PDCLs poly-L-lysine/polyethylene-glycol (PLL-PEG) was added to the media at 10 μM to reduce cell- clumping and sticking to microchannel walls. Clumps of cells, visualized through a microscope during measurement, were excluded from measurement in the SMR. The system and cells were kept in culturing conditions (5% CO_2, 37 °C) for all measurements as previously described[12].

Flow cytometry. All flow cytometry measurements were performed on a BD LSR II (BD Biosciences) using 4′,6-diamidino-2- phenylindole (DAPI) (BioLegend, Cat#422801) and Annexin V (BioLegend, Cat#640907).

31. Klco, J.M. *et al*. Genomic impact of transient low-dose decitabine treatment on primary AML cells. *Blood* **121**, 1633–1643 (2013).

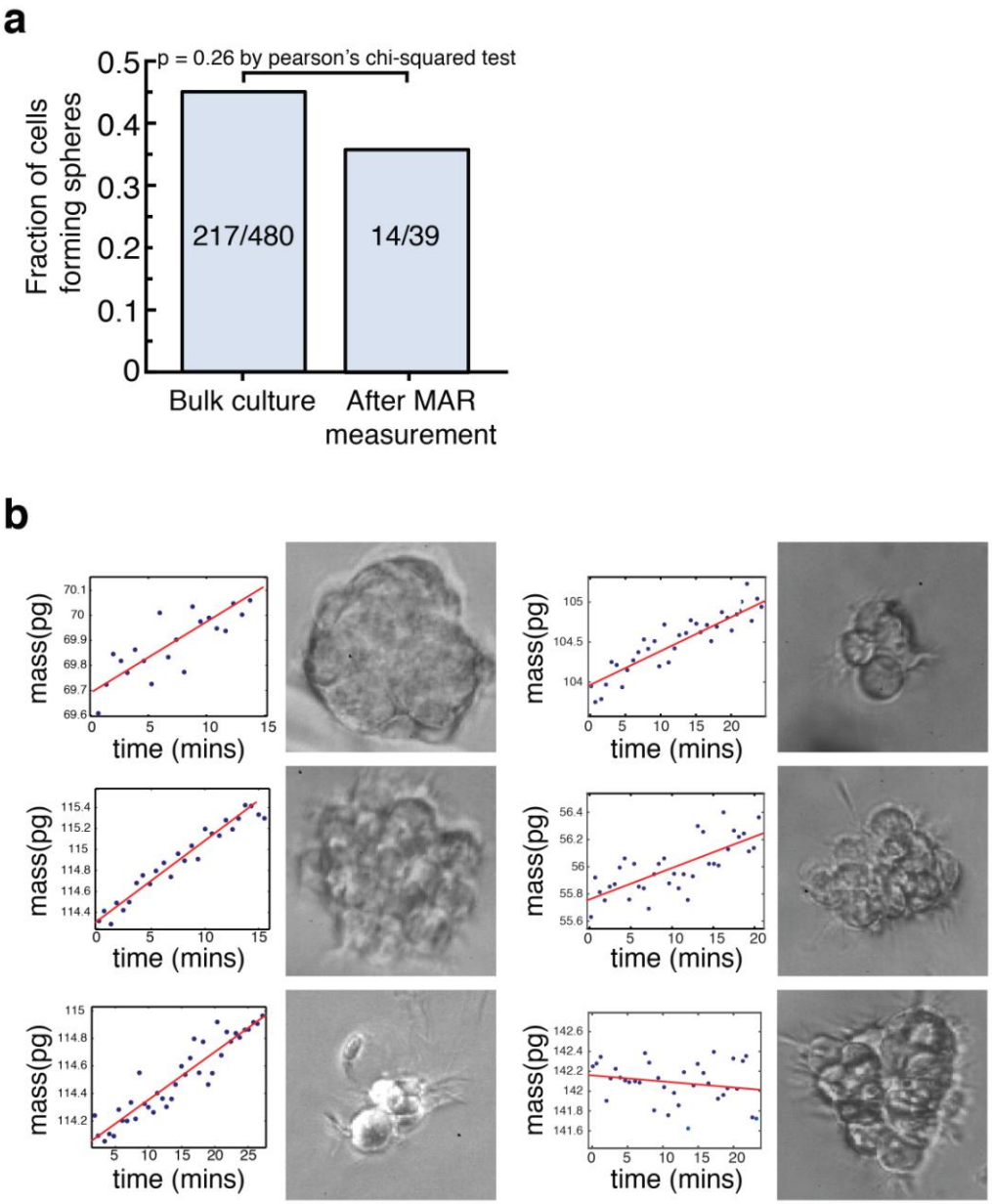

Supplementary Figure 1

Sphere forming assay of BT145 GBM PDCL

(a) Sphere forming potential of single BT145 GBM cells isolated from bulk culture or SMR post-MAR measurement. p-values reflect output of Pearson's chi-squared test. **(b)** Representative single-cell trajectories paired with images of sphere forming potential 2-weeks after measurement. Note that even cells with minimal or negative growth over the 15-minute period may retain tumorsphere-forming potential (bottom right).

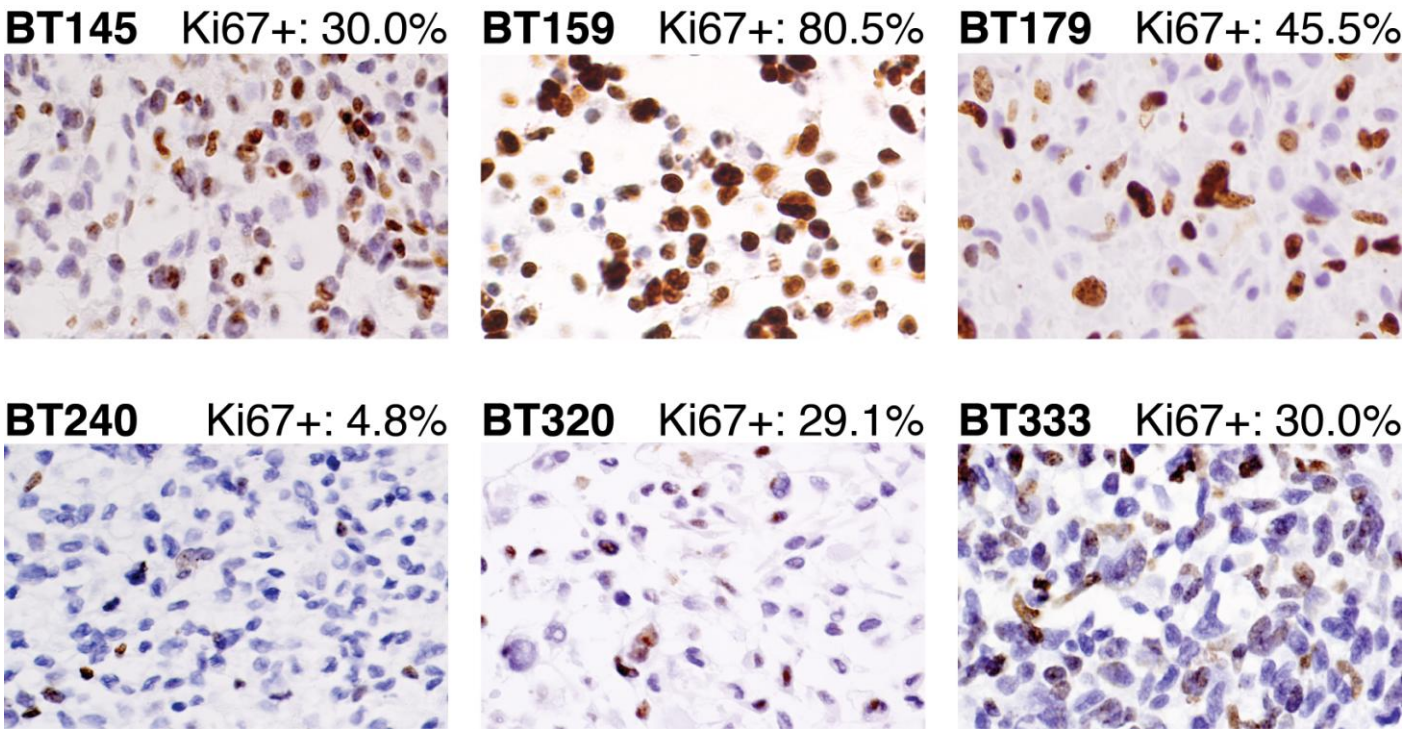

Supplementary Figure 2

Growth heterogeneity maintained across multiple passages of PCDLs

Representative staining results from immunohistochemistry for Ki67 on BT145, BT159, BT179, BT240, BT320, and BT333 cell lines. Results quantified as percentage of total cells stained positive.

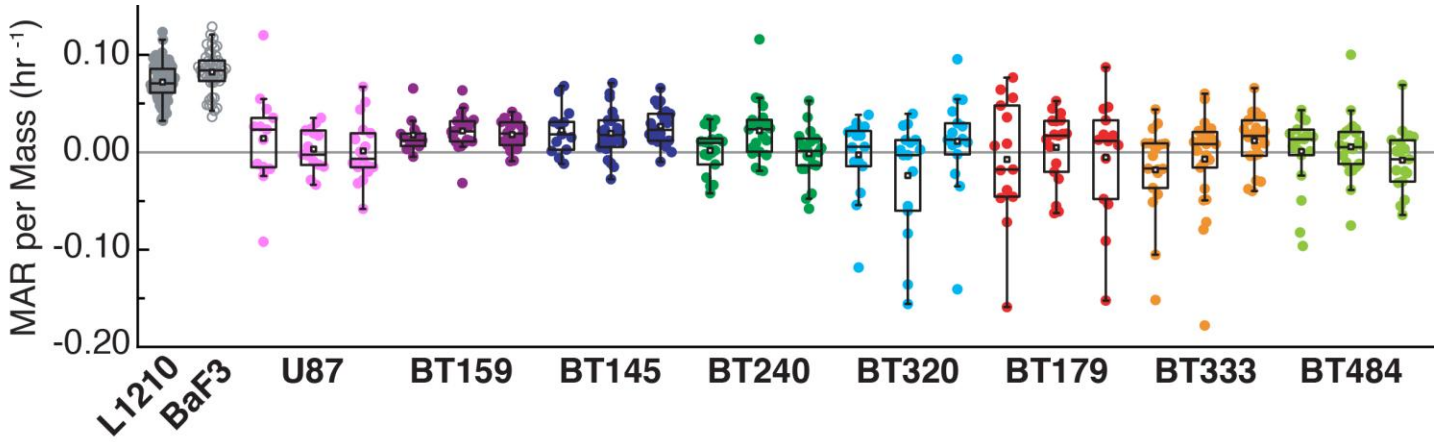

Supplementary Figure 3

Growth heterogeneity maintained across multiple passages of PCDLs

Box plot comparison of MAR normalized to mass for the same cell lines as in Figure 1c with three passages of GBM-PDCLs shown separately. Boxes represent the inter-quartile range and white squares the average of all measurements. From left to right, n = 84; 46; 13, 14, 17; 12, 21, 18; 21, 18, 13; 19, 21, 21; 16, 16, 16; 14, 18, 14; 18, 25, 21; 19, 22, 18.

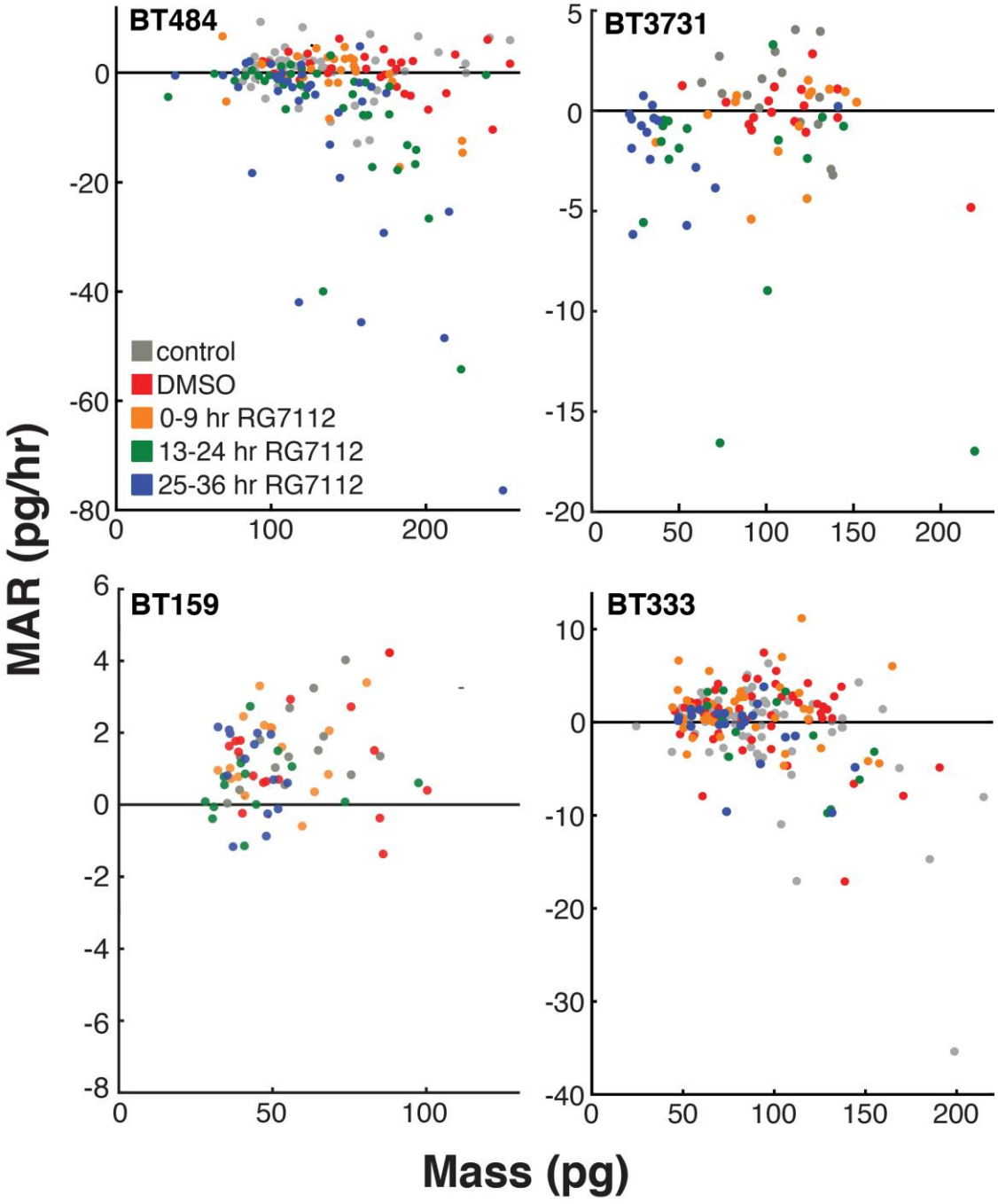

Supplementary Figure 4

PDCLs following treatment with MDM2 inhibitor RG7112

Scatter plots of MAR versus mass for BT484, BT3731, BT159, BT333 cells following treatment with 1 μM RG7112.

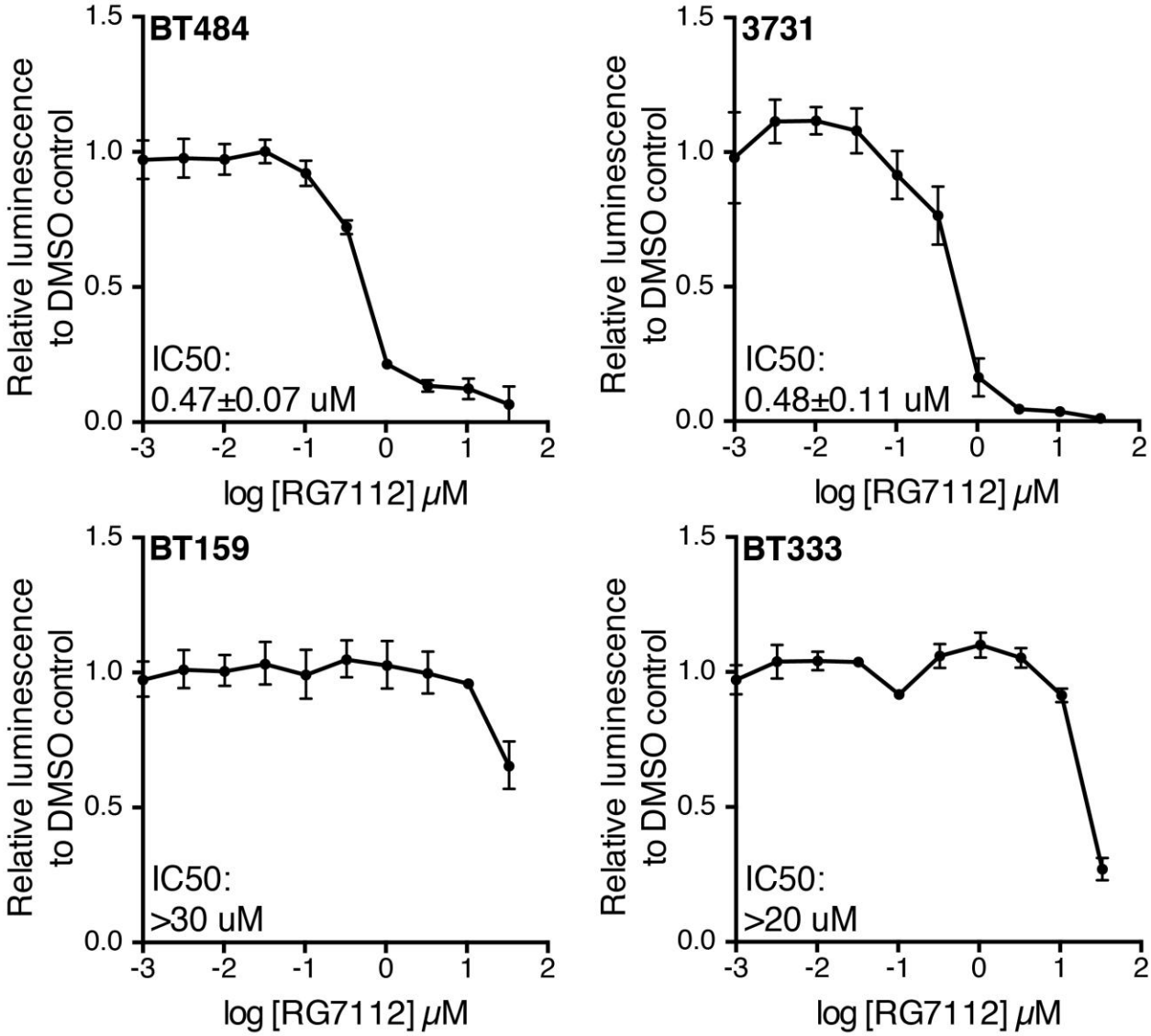

Supplementary Figure 5

Dose-response curves for GBM PDCLs treated with RG7112

Curves from PDCLs were generated using CellTiter-Glo at 72 hrs, following treatment with 1 μM RG7112. IC50 values embedded in each graph reflect the output of a four parameter nonlinear regression model +/- the range of the 95% confidence interval.

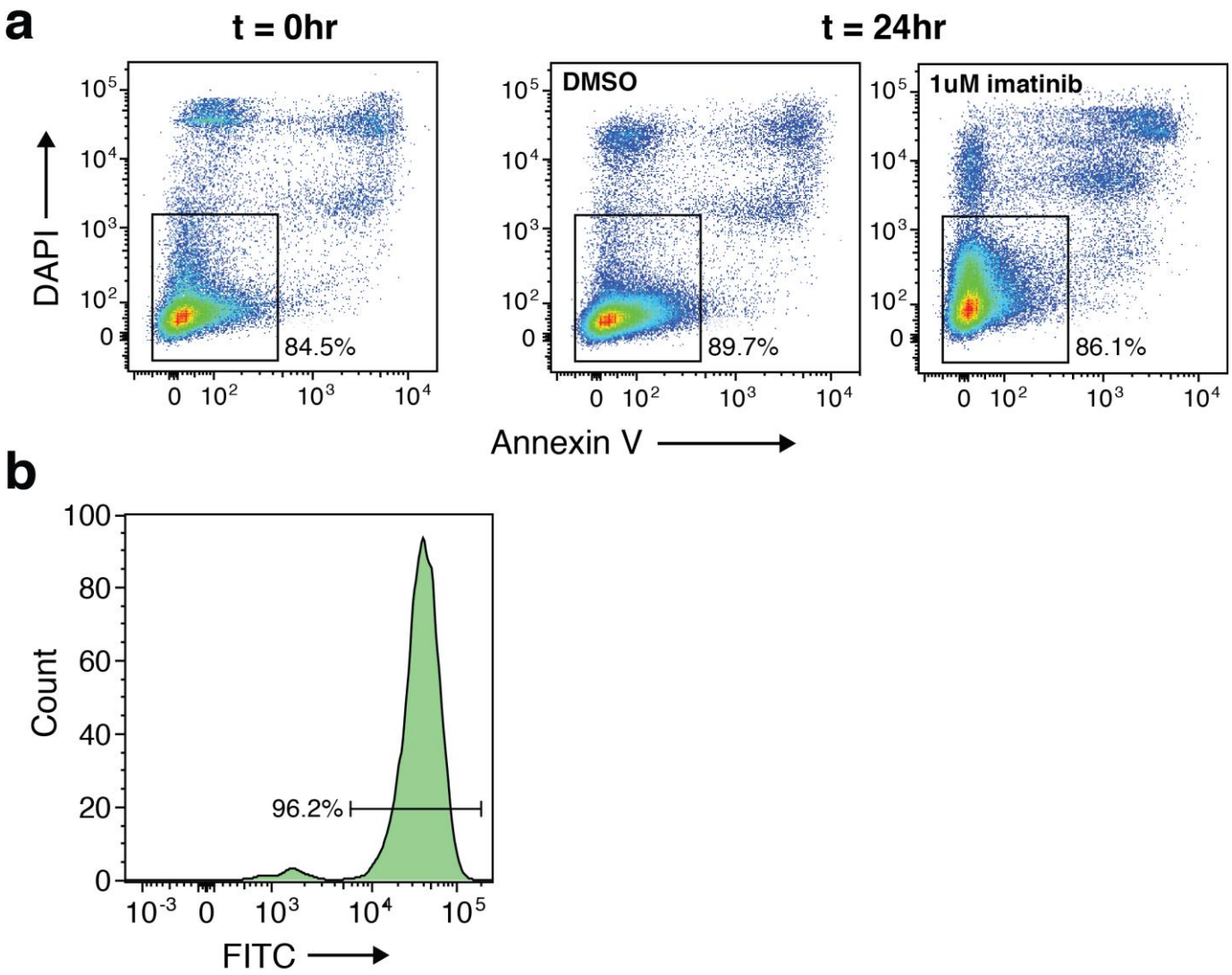

Supplementary Figure 6

Viability and purity of primary murine B-ALL by flow cytometry

(a) Representative dot plots of cells stained with DAPI and Annexin V, as markers of viability. **(b)** Representative histogram of GFP expression after cell sorting. Leukemia cells in this model uniquely express GFP. FACS analysis was performed on all primary murine splenocyte samples.

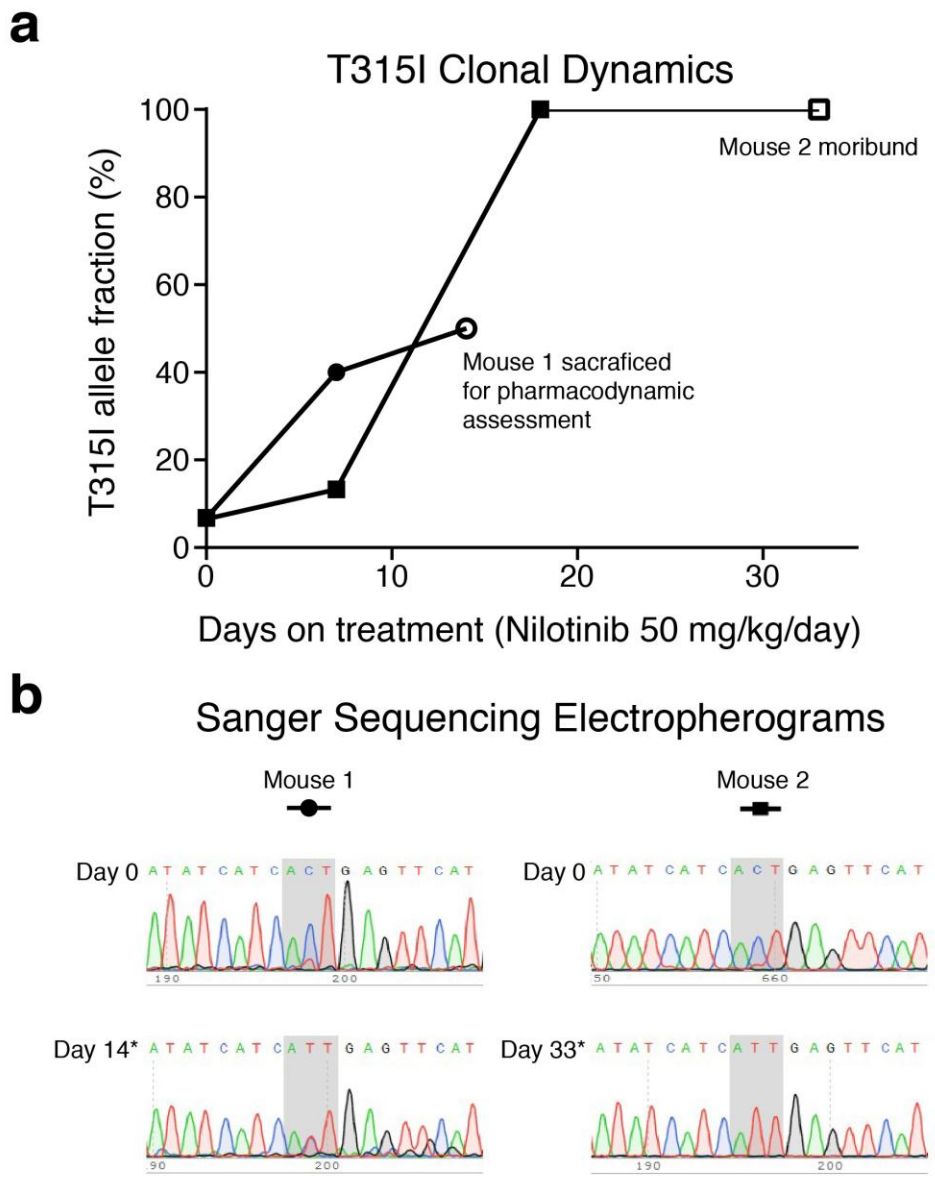

Supplementary Figure 7

In vivo clonal dynamics in a transgenic murine model of BCR-ABL B-ALL

(a) The allelic frequency of BCR-ABL T315I in two mice treated with nilotinib, a surrogate for imatinib. Allelic frequencies were calculated by visual measurement of the relative heights of the electropherogram peaks; values from the paired forward and reverse sequencing phases were averaged to produce the allelic frequencies shown. Mouse 1 (closed circles) was sacrificed on day 14 for routine pharmacodynamic assessment (open circle). Mouse 2 (closed squares) was sacrificed after developing clinical signs of advanced leukemia on day 33 (open square). **(b)** Representative electropherograms showing ABL codon 315 (in gray; ACT indicates wild type T315, and ATT indicates the point mutation T315I). As demonstrated, the mutant subclone expands in relation to WT during treatment with nilotinib, to which WT but not T315I BCR-ABL is sensitive.

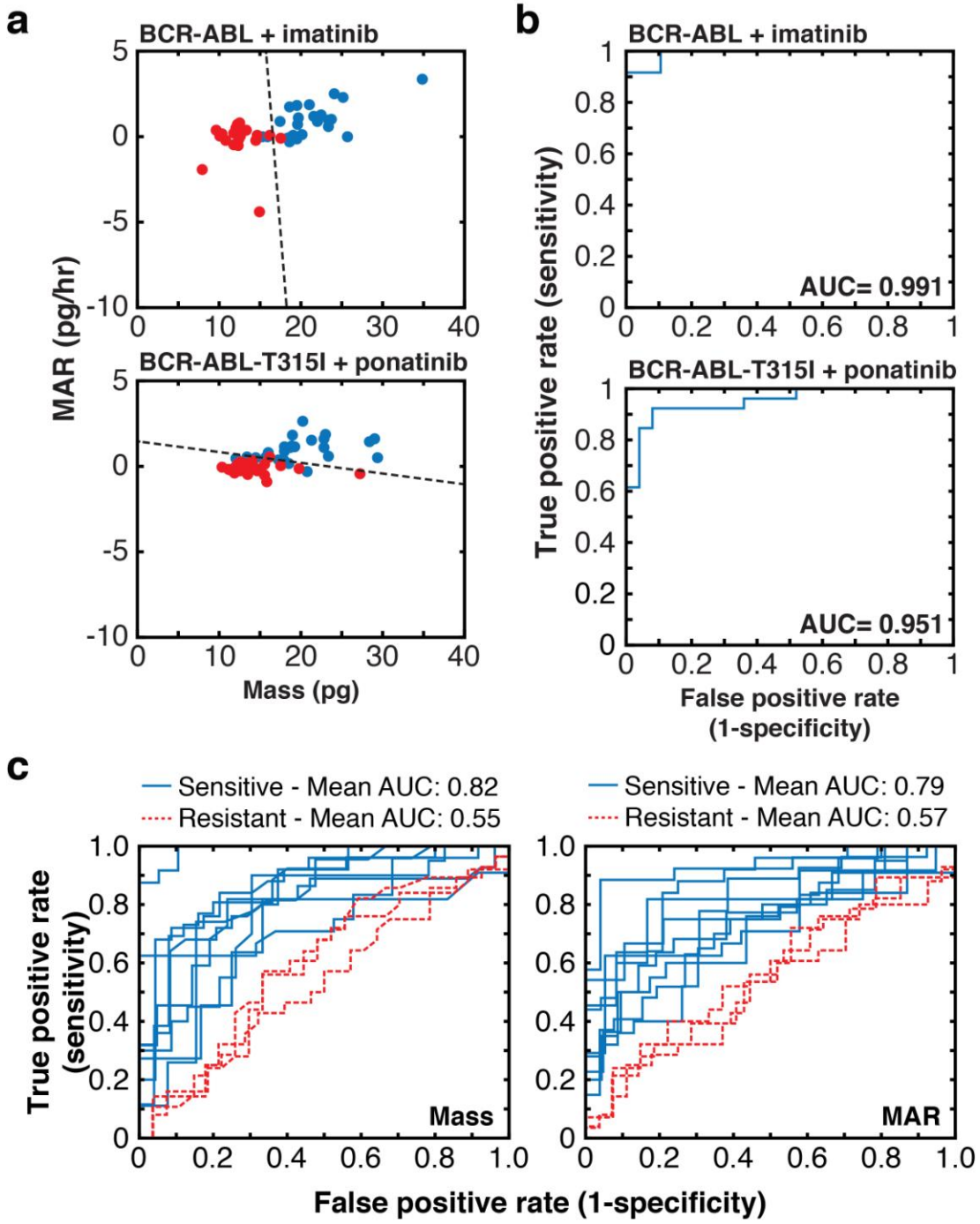

Supplementary Figure 8

MAR or mass can be used individually as a classifier for drug susceptibility

Primary murine BCR-ABL ALL and BCR-ABL T315I ALL cells treated with 1 μM imatinib, or 100 nM ponatinib, respectively. **(a)** MAR versus mass plot with overlay of an orthogonal vector (dotted line) designating the threshold resulting from LDA. Cells treated with drug are in red, and DMSO control cells are blue **(b)** ROC curves from same paired control and treatment data following LDA of MAR per mass plot. **(c)** Overlaid ROC curves of paired control and treatment data for all treatment replicates using only mass or MAR parameter. Cells treated with therapy to which they are sensitive or resistant are shown with blue solid lines or red dotted lines, respectively.

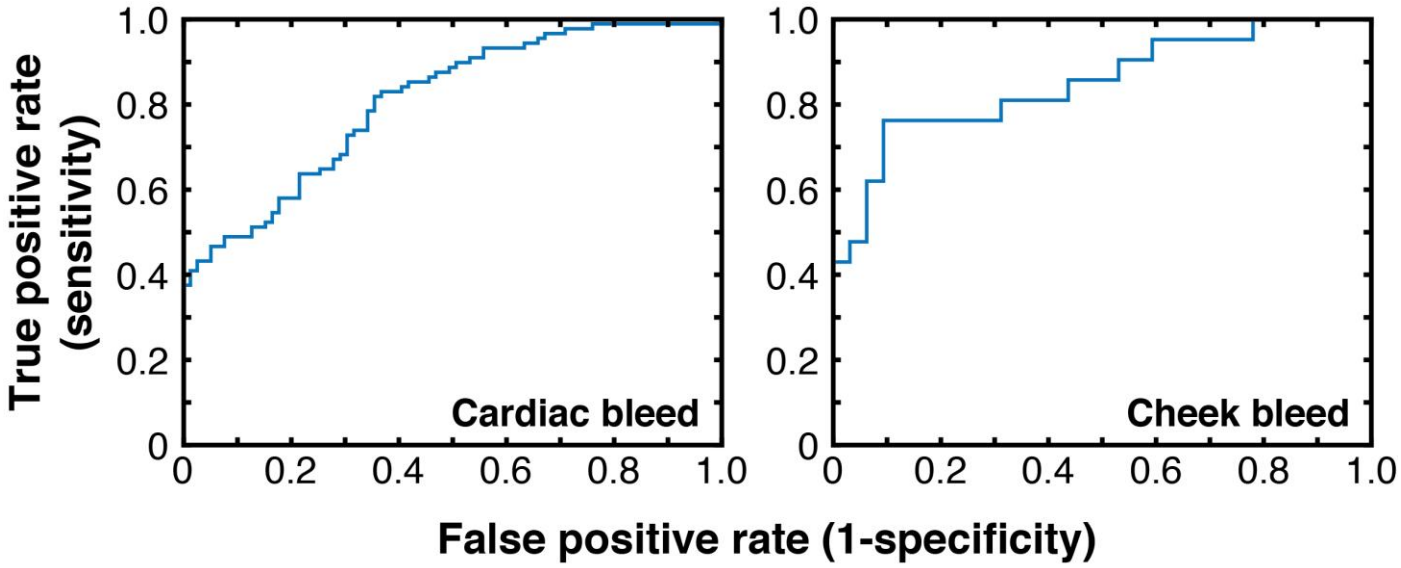

Supplementary Figure 9

Predictive power of MAR for cells isolated from circulation

Primary murine BCR-ABL T315I cells isolated from circulation, treated with DMSO or 100 nM ponatinib. ROC curves of paired control and treatment data for each replicate following LDA.

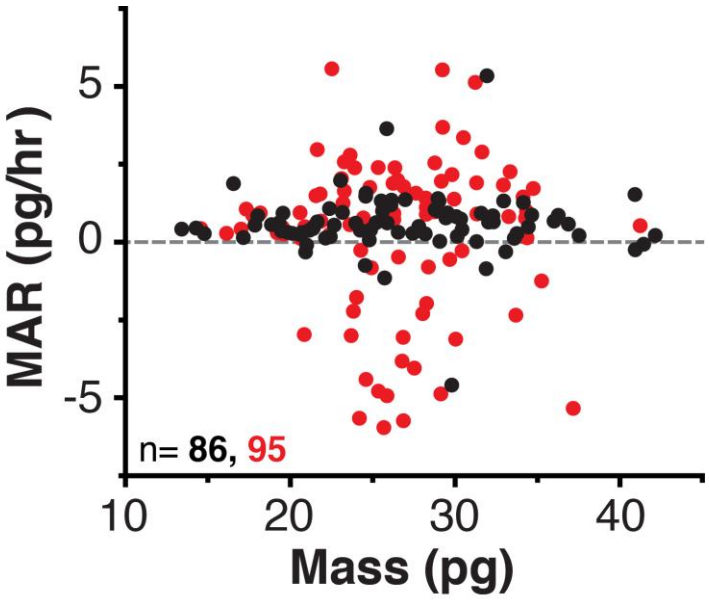

Supplementary Figure 10

Patient sample treated *in vivo* shows consistent reduction in MAR

MAR versus Mass plot for blasts from peripheral blood samples of AML. Pre-treatment sample shown in black (n=86), and sample obtained after the patient received 48 hrs of of treatment with an experimental MDM2 inhibitor shown in red (n=95).

PDCL	Diagnosis	EGFR	CDK4	CDK6	PTEN	PDGFRA	MET	CDKN2A	NF1	MDM2	RB1	TP53
BT145	GBM Astrocytoma IV	WT	WT	WT	WT	WT	WT	HOMDEL	WT	WT	WT	WT
BT159	GBM Astrocytoma IV	WT	WT	WT	WT	WT	WT	HOMDEL	MUT p.D176E	WT	WT	WT
BT179	GBM Astrocytoma IV	AMP	WT	WT	L70_splice	WT	WT	HOMDEL	WT	WT	WT	MUT p.I255T
BT239	GBM Astrocytoma IV	Mut p.R521K	WT	WT	WT	WT	WT	HOMDEL	MUT L249fs	WT	WT	WT
BT240	GBM Astrocytoma IV	WT	WT	WT	WT	WT	WT	HOMDEL	WT	WT	WT	MUT p.S227Y
BT320	GBM Astrocytoma IV	WT	WT	WT	MUT p.G132A	WT	WT	HOMDEL	WT	WT	WT	HOMDEL
BT333	GBM Astrocytoma IV	AMP, MUT p.F254I	WT	WT	WT	WT	WT	HOMDEL	MUT p.D176E	WT	WT	MUT p.V173M
BT484	GBM Astrocytoma IV				MUT p.C136Y					AMP		WT
3731	GBM Astrocytoma IV									AMP		WT

Supplementary Table 1

GBM PDCL mutation analysis

Abbreviations: AMP, amplification; MUT, mutation; HOMDEL, homozygous deletion.